Full Waveform Tomography for the upper South Island region, New Zealand

Trung Dung (Andrei) Nguyen,
Robin Lee,
Brendon Bradley,
Robert Graves

Christchurch, Oct. 22nd 2020

Motivation of full waveform tomography

- Iteratively improve an initial regional velocity model (created by travel time tomography).
- Utilize full information of the broadband station data/ CMT catalogue solutions of the local earthquake events and the numerical solution of the visco-elastic wave propagation/ computational capability from Nesi.
- Aim to improve the ground motion simulation predictions.

3-D Velocity Model and Earthquake Ground Motions for the upper South Island region, NZ

- Initial model: Eberhart-Phillips NZVM models 2010 and 2020 integrated from several regional velocity studies using local earthquakes and onshore recordings of offshore active source data.
- The region examined in this study is the upper South Island (and Wellington at the bottom of the North Island), as shown in Figure 1.

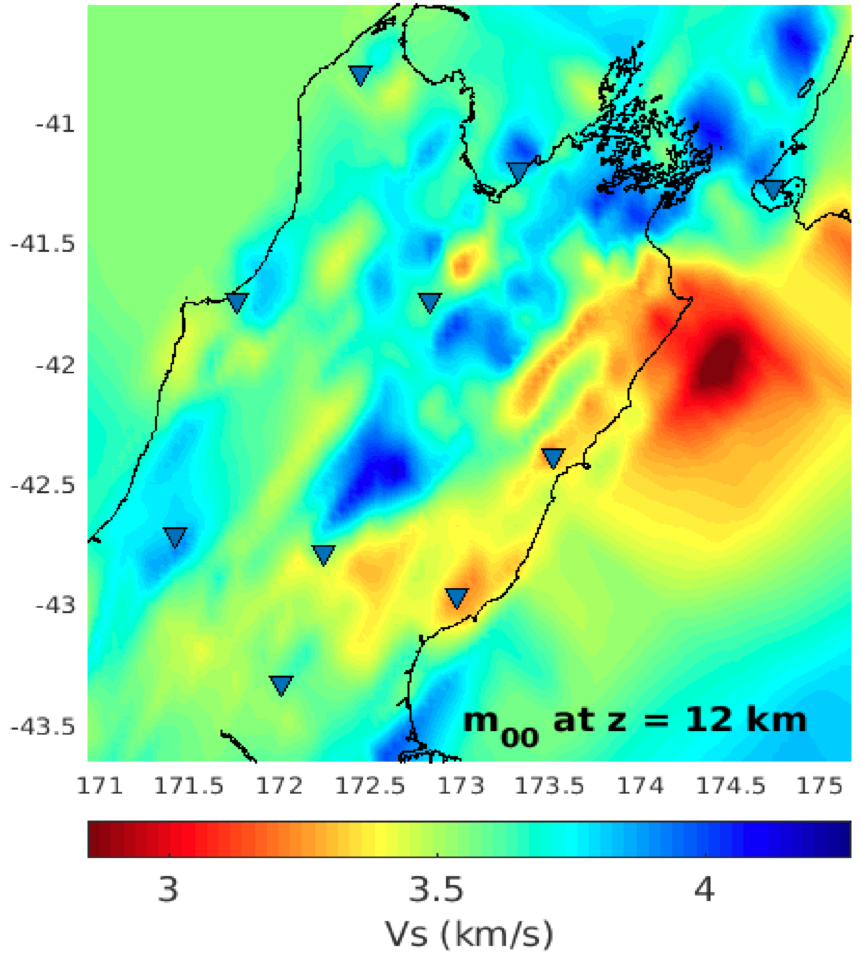

Figure 1: NZVM 2010 model for Vs

3-D Velocity Model and Earthquake Ground Motions for the upper South Island region, NZ

- Ground motions utilized in the waveform inversion are obtained from the FDSN GeoNet channel. From a candidate set of 82 earthquakes, 13 were selected for model training (Figure 2).
- The source models for these events were obtained from the GeoNet centroid moment tensor solution catalogue (Ristau, 2008, 2013).

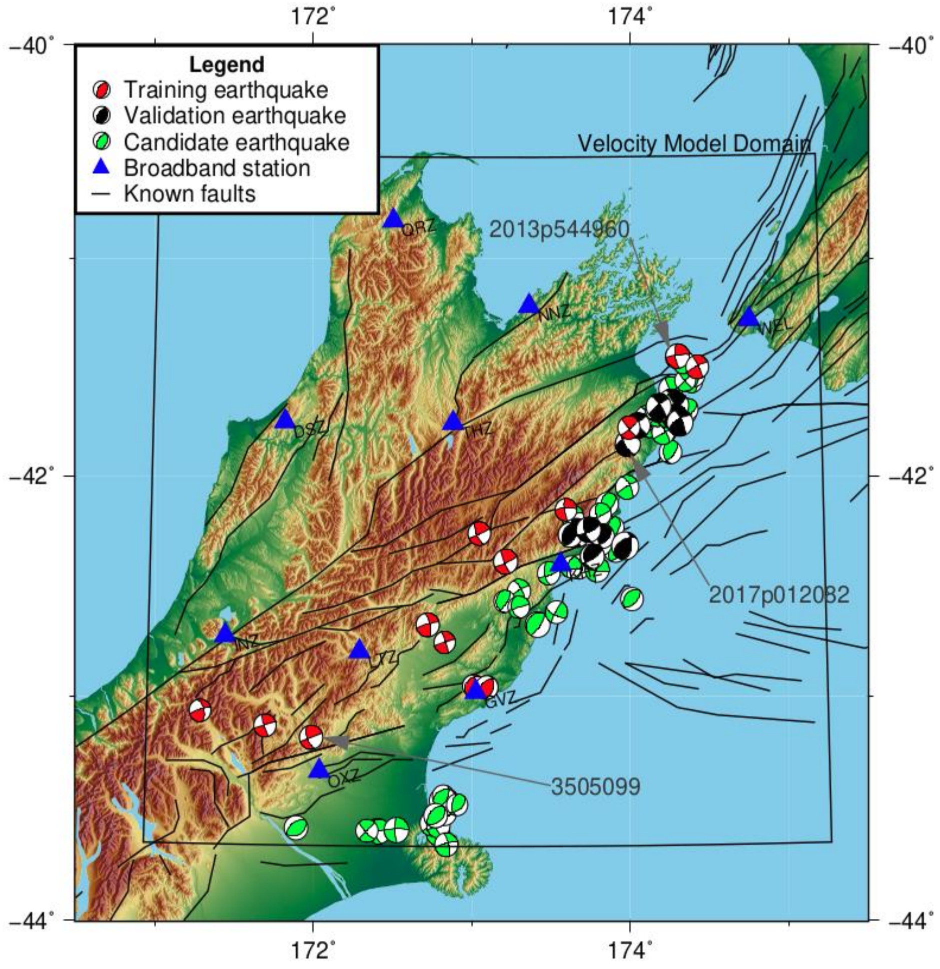

Figure 2: Broadband stations and earthquake events in the upper South Island

Tomographic inversion using adjoint method: methodology

- Fully automated workflow and parallelization for multi-events inversion (Figure 3).

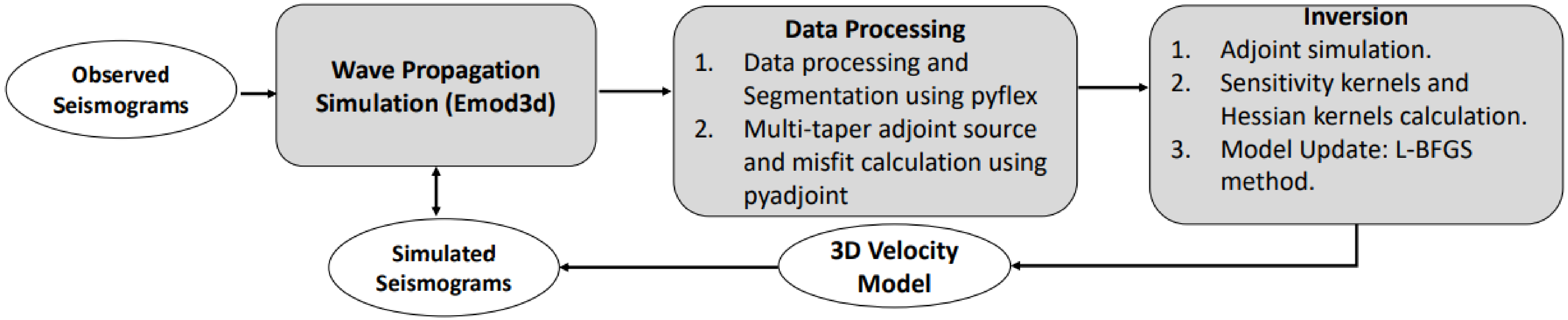

Figure 3: Computational workflow of Full Waveform Inversion (FWI)

Data processing packages

- *Pyflex* for waveform segmentation

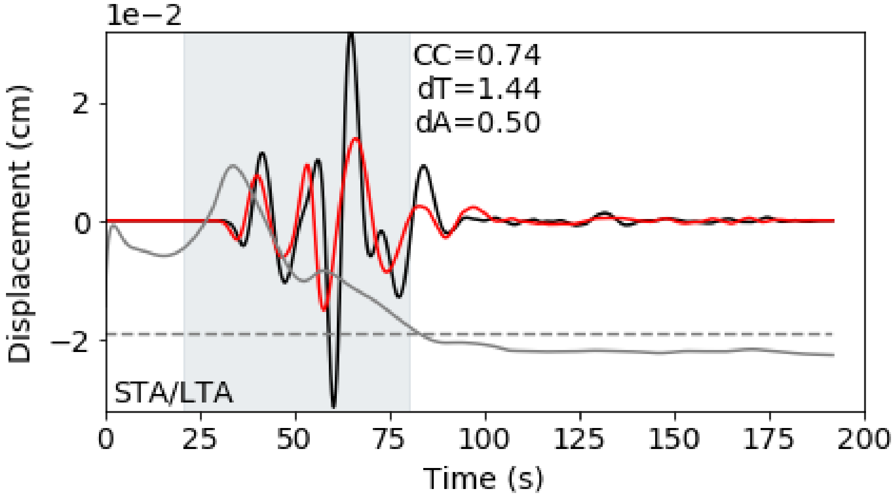

Figure 4: window picked by *Pyflex*

Data processing packages

- *Pyadjoint* for calculation of adjoint source/ multi-taper misfit

$$\chi_p(\mathbf{m}) = \frac{1}{N_s}\sum_{i=1}^{N_s}\frac{1}{N_i}\sum_{j=1}^{N_i}\frac{1}{2}\int_{-\infty}^{\infty} W_{p_{ij}}(\omega)\left[\frac{\tau_{ij}^d(\omega)-\tau_{ij}^s(\omega,\mathbf{m})}{\sigma_p(\omega)}\right]^2 d\omega$$

(a)

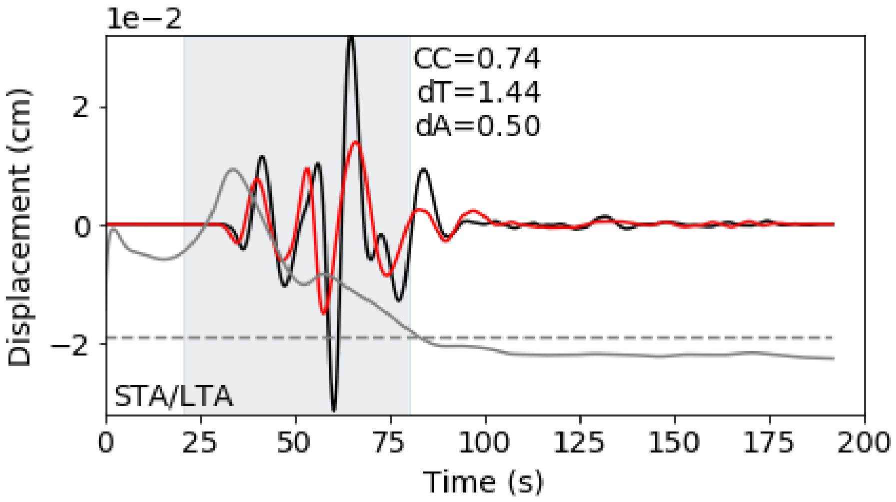

(b)

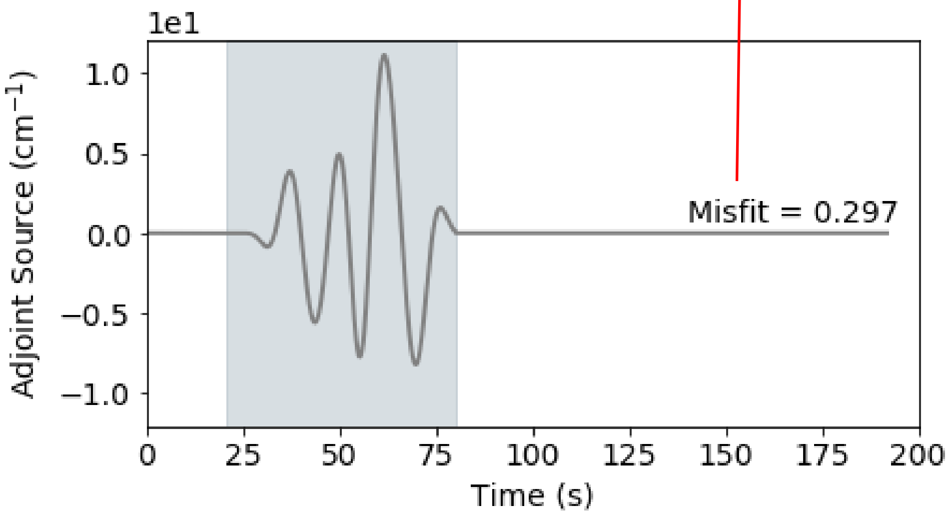

Figure 4: (a) window picked by *Pyflex*, (b) adjoint source construction and misfit measurement by *Pyadjoint*

Data processing packages

- *Pyadjoint* for calculation of adjoint source/ multi-taper misfit

$$\chi_p(\mathbf{m}) = \frac{1}{N_s}\sum_{i=1}^{N_s}\frac{1}{N_i}\sum_{j=1}^{N_i}\frac{1}{2}\int_{-\infty}^{\infty} W_{p_{ij}}(\omega)\left[\frac{\tau_{ij}^{d}(\omega)-\tau_{ij}^{s}(\omega,\mathbf{m})}{\sigma_p(\omega)}\right]^2 d\omega$$

(a)

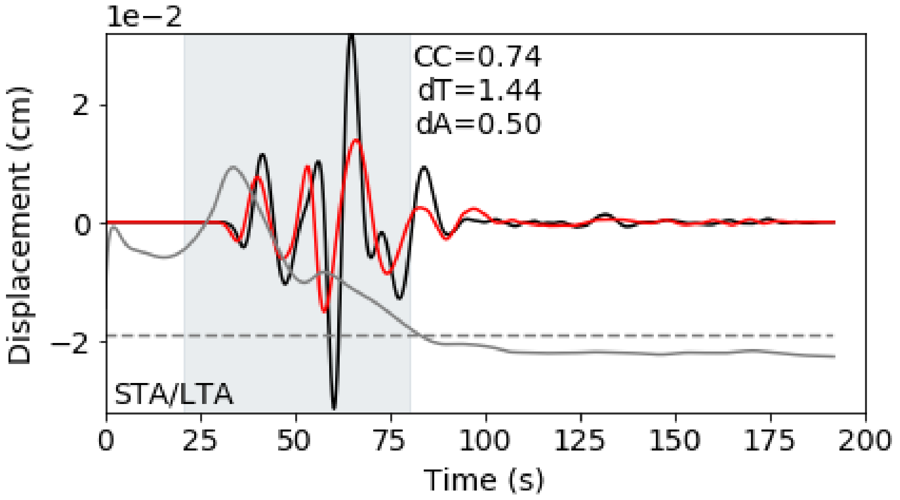

(b)

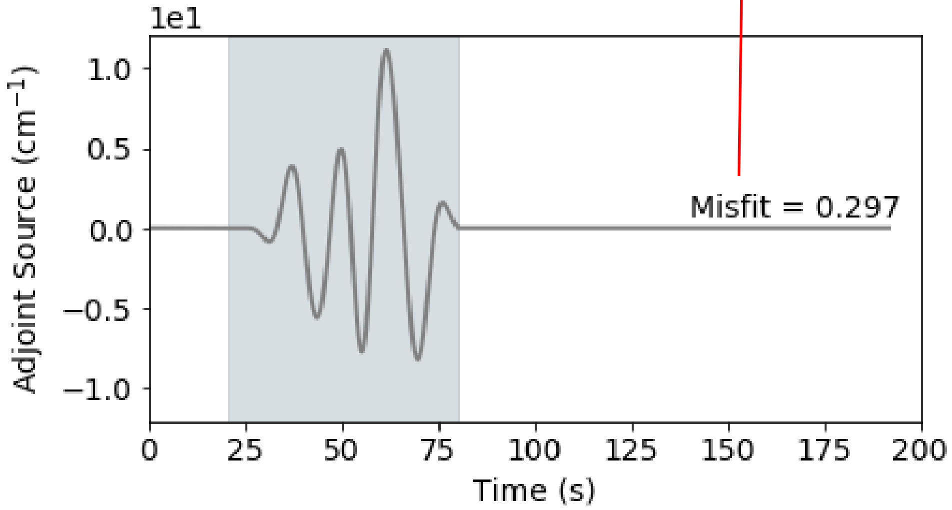

Figure 4: (a) window picked by *Pyflex*, (b) adjoint source construction and misfit measurement by *Pyadjoint*

- Other measurements: relative waveform misfit *(RWM)* and travel time difference *(ΔT)*

$$RWM = \frac{\int_{t_0}^{t_1}\left[d(t)-s(t)\right]^2 dt}{\sqrt{\int_{t_0}^{t_1} d^2(t)dt\int_{t_0}^{t_1} s^2(t)dt}} \qquad NCC = \frac{\int_{t_0}^{t_1} d(t-\Delta T)s(t)dt}{\sqrt{\int_{t_0}^{t_1} d^2(t-\Delta T)dt\int_{t_0}^{t_1} s^2(t)dt}}$$

Adjoint simulation and sensitivity kernel calculation

- Adjoint simulation: back-propagating the difference b/w observed and synthetic data (adjoint source) at station's locations.

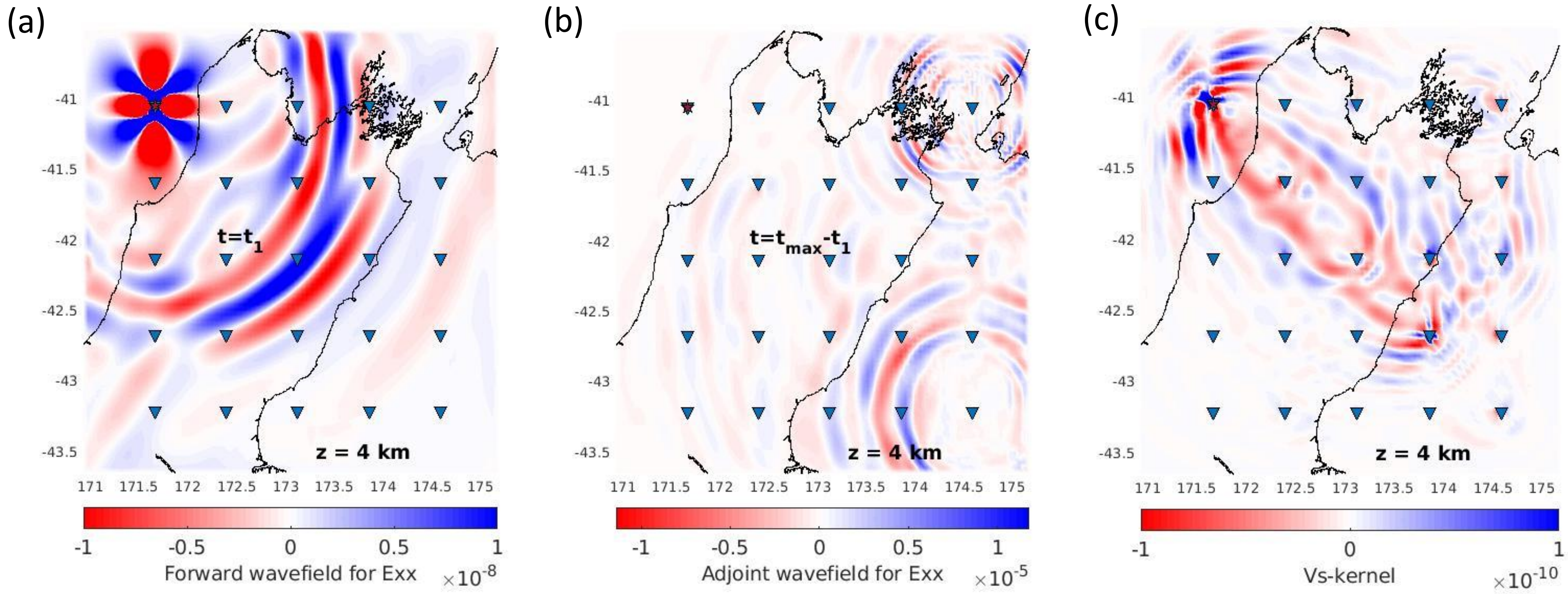

Figure 5: (a) forward wavefield, (b) adjoint wavefield, (c) sensitivity kernel for Vs

Data processing packages and verification via synthetic checkerboard test

- Synthetic checkerboard test: setup.
  https://wiki.canterbury.ac.nz/display/QuakeCore/Check+board+using+16+srf+synthetic+sources+and+25+stations

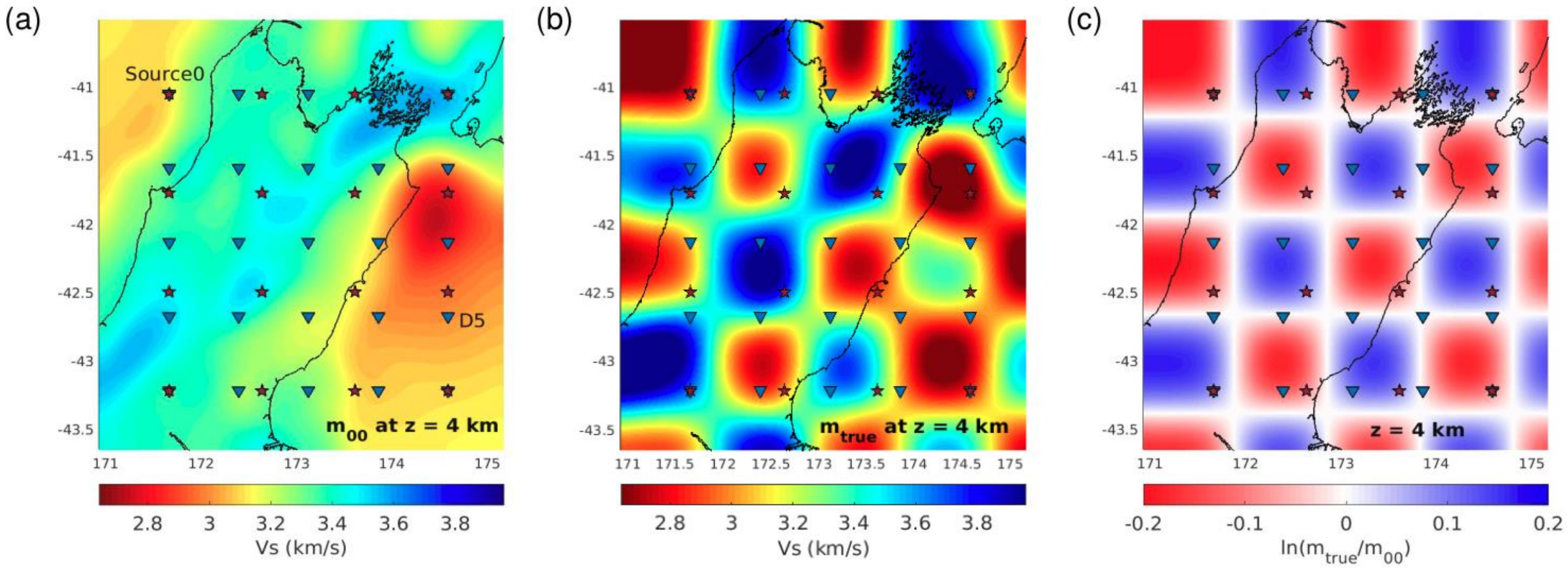

Figure 6: Checkerboard test setup: (a) Initial model, (b) True model, (c) Difference between true and initial model ln(mTrue/m00)

Data processing packages and verification via synthetic checkerboard test

- Synthetic checkerboard test: results.

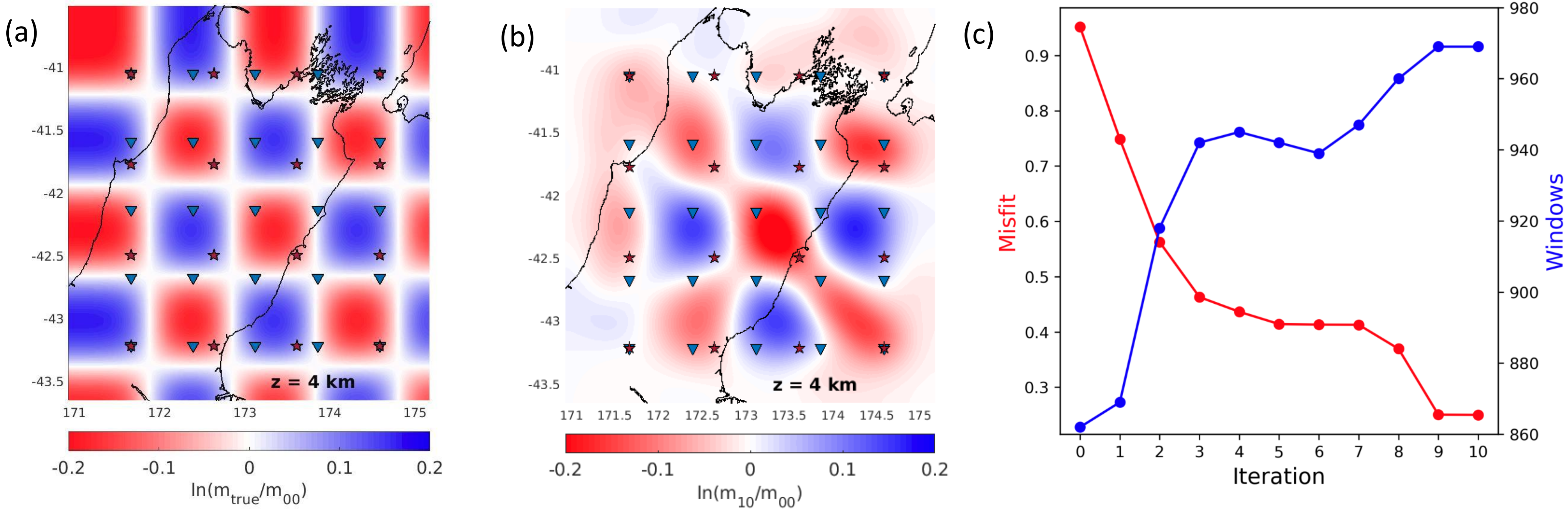

Figure 8: Checkerboard test results: (a) Difference between true and initial model ln(mTrue/m00) (checkerboard), (b) recover of the checkerboard after 10 iteration, (c) Misfit and windows picked along iterations.

Full Waveform Tomography using broadband station data: first inversion run using 13 events

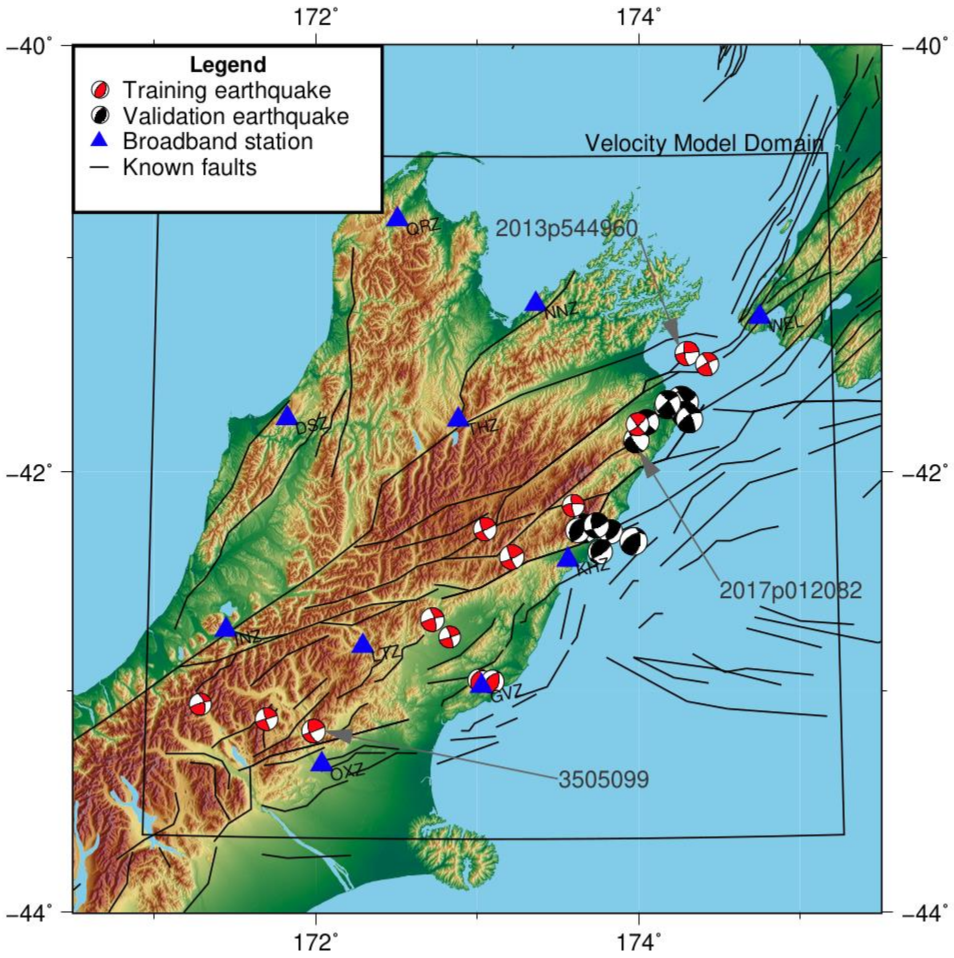

Figure 9: : Broadband stations and earthquake events included in the tomographic study

Full Waveform Tomography using broadband station data: first inversion run using 13 events

Multi-taper misfit reduction and mean values of *RWT* and *dT* along iterations

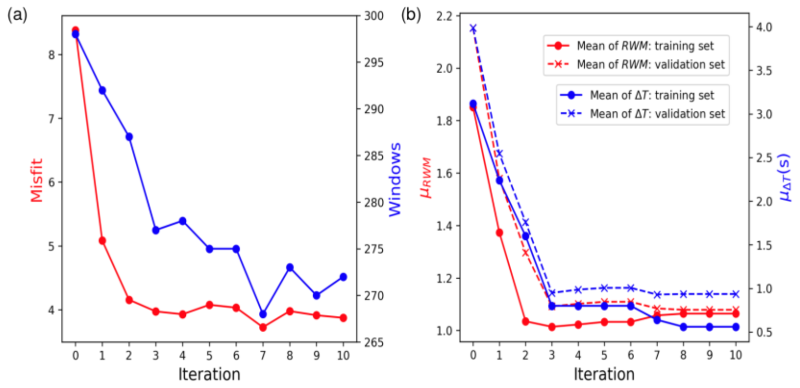

Figure 10: (a) Change of misfit (red) and number of windows (blue) along the first inversion; (b) Change of mean for *RWM* (red) and mean for *dT* (blue) for the training set (solid) and the validation set (dashed).

Multi-taper misfit reduction and mean values of *RWT* and *dT*

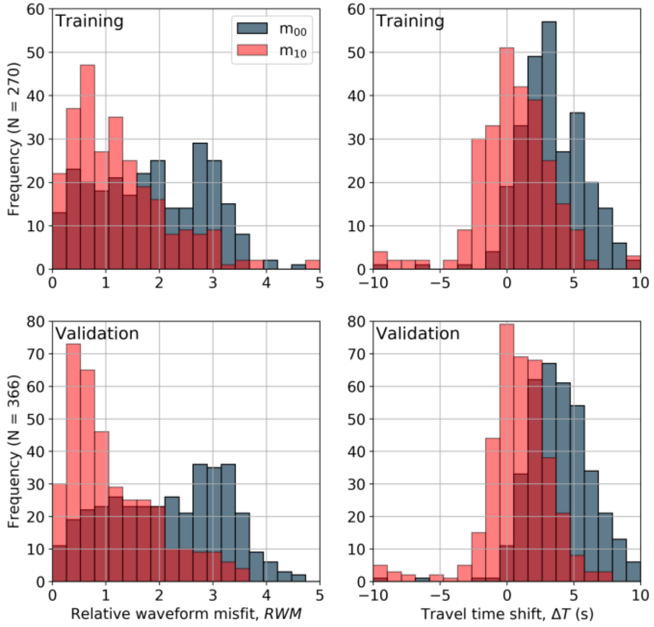

Figure 11: Histograms for *RWM* and *dT* for 27 events data for models m10 (grey) and m15 (red) for the training set (top) and validation set (bottom).

Full Waveform Tomography using broadband station data: second run using 27 events

Multi-taper misfit reduction and mean values of *RWT* and *dT* along iterations

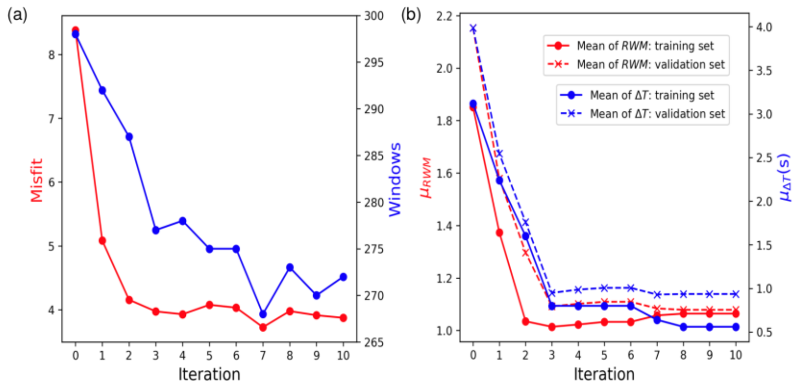

Figure 10: (a) Change of misfit (red) and number of windows (blue) along the first inversion; (b) Change of mean for *RWM* (red) and mean for *dT* (blue) for the training set (solid) and the validation set (dashed).

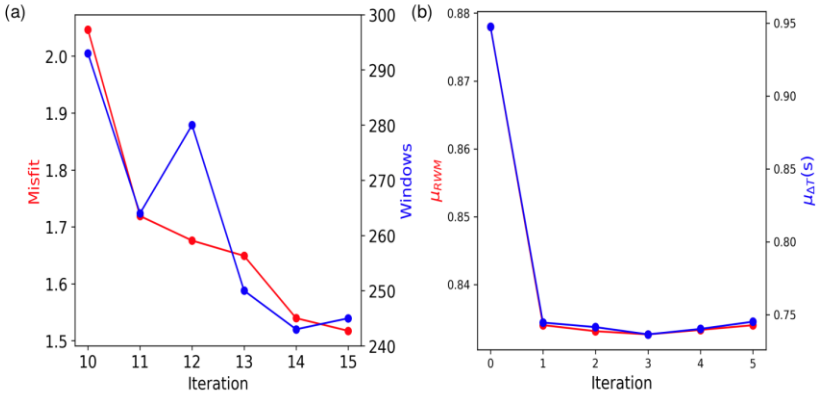

Figure 12: (a) Change of misfit (red) and number of windows (blue) along the second inversion; (b) Change of mean for *RWM* (red) and mean for *dT* (blue).

Multi-taper misfit reduction and mean values of *RWT* and *dT*

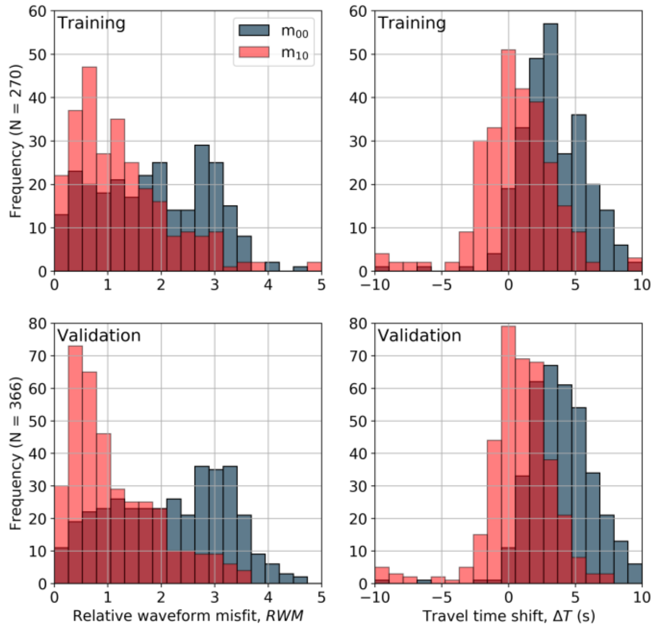

Figure 11: Histograms for *RWM* and *dT* for 27 events data for models m10 (grey) and m15 (red) for the training set (top) and validation set (bottom).

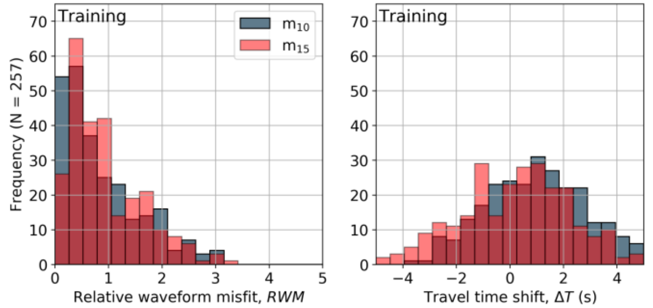

Figure 13: Histograms for *RWM* and *dT* for 27 events data for models m10 (grey) and m15 (red).

Full Waveform Tomography using broadband station data: model updating at the first inversion run using 13 events

Figure 14: Model change after 10 iterations at depth: (a) 4 km, (b) 12 km and (c) 20 km.

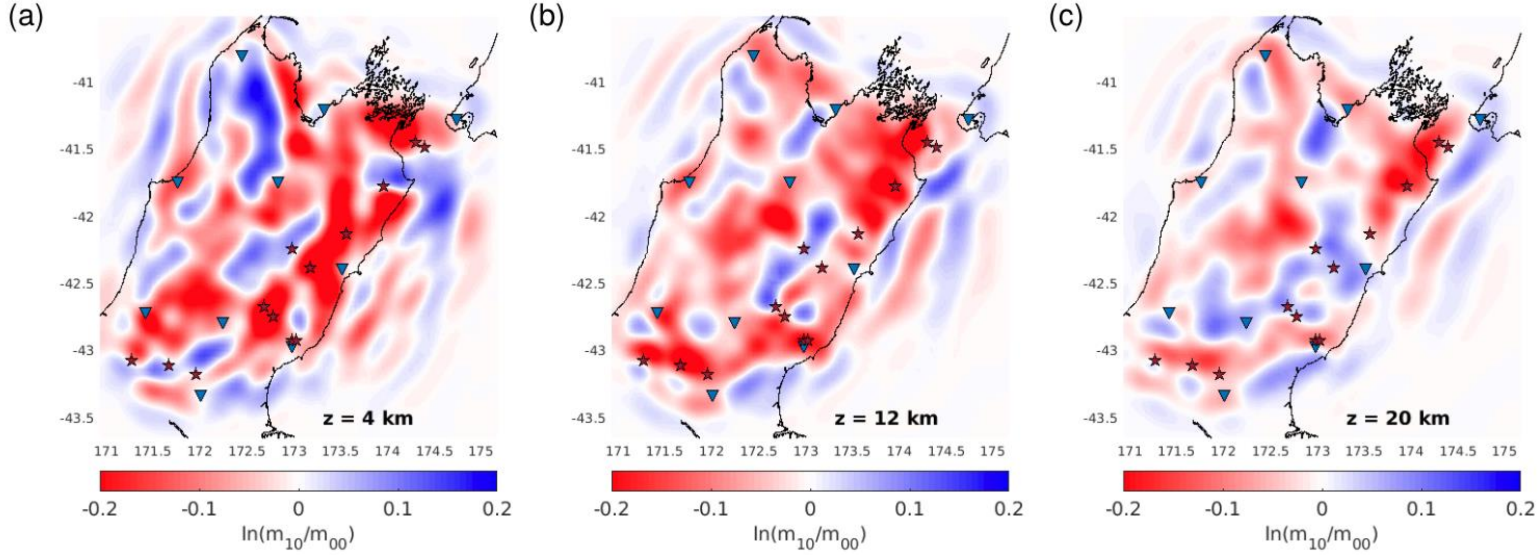

Figure 15: Inverted model after 10 iterations at depth: (a) 4 km, (b) 12 km and (c) 20 km.

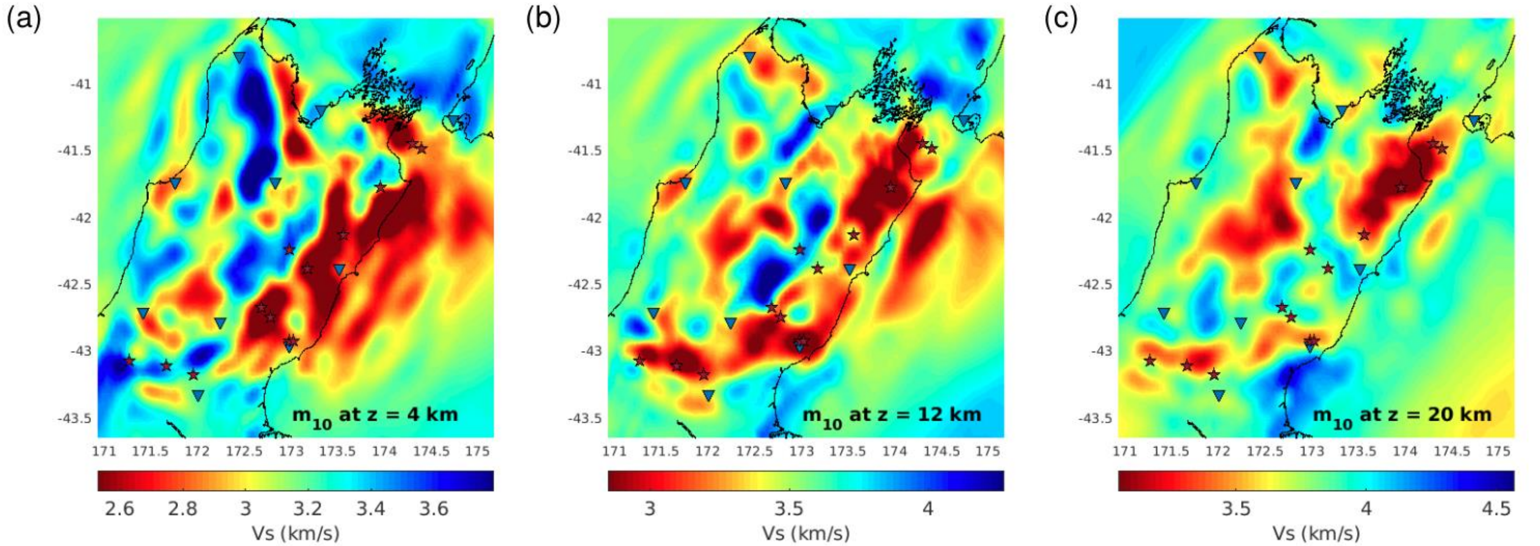

Full Waveform Tomography using broadband station data: model updating at the second run using 27 events

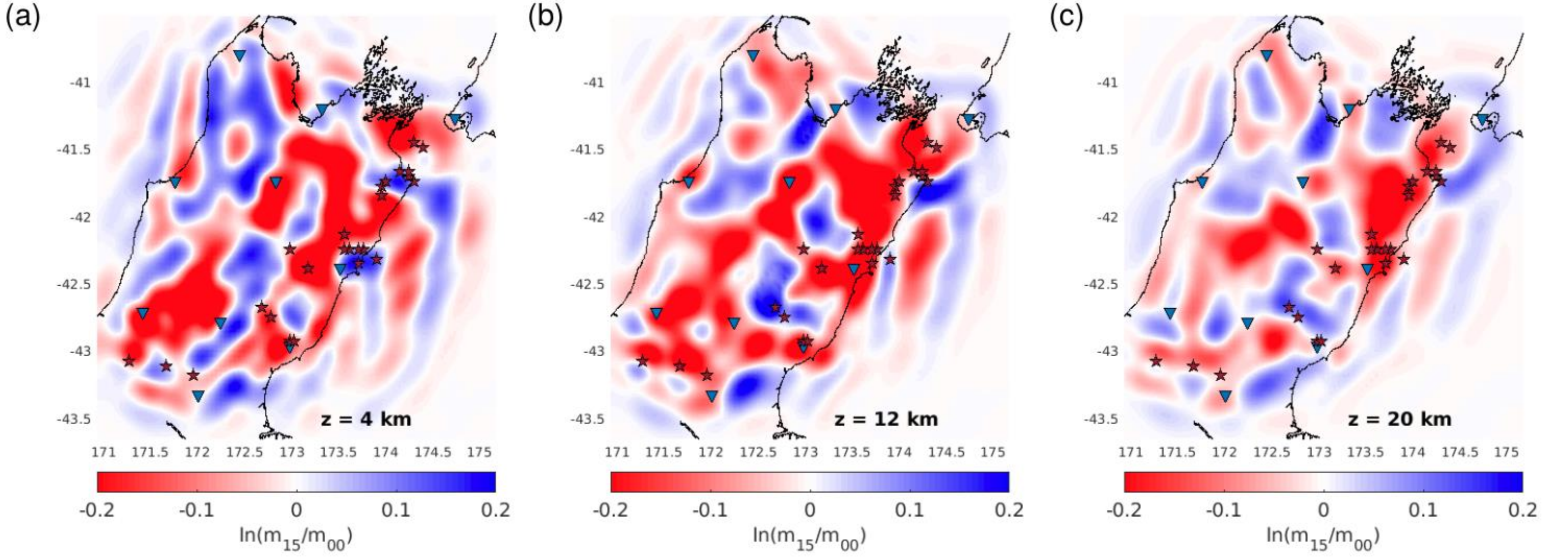

Figure 16: Model change after 15 iterations at depth: (a) 4 km, (b) 12 km and (c) 20 km.

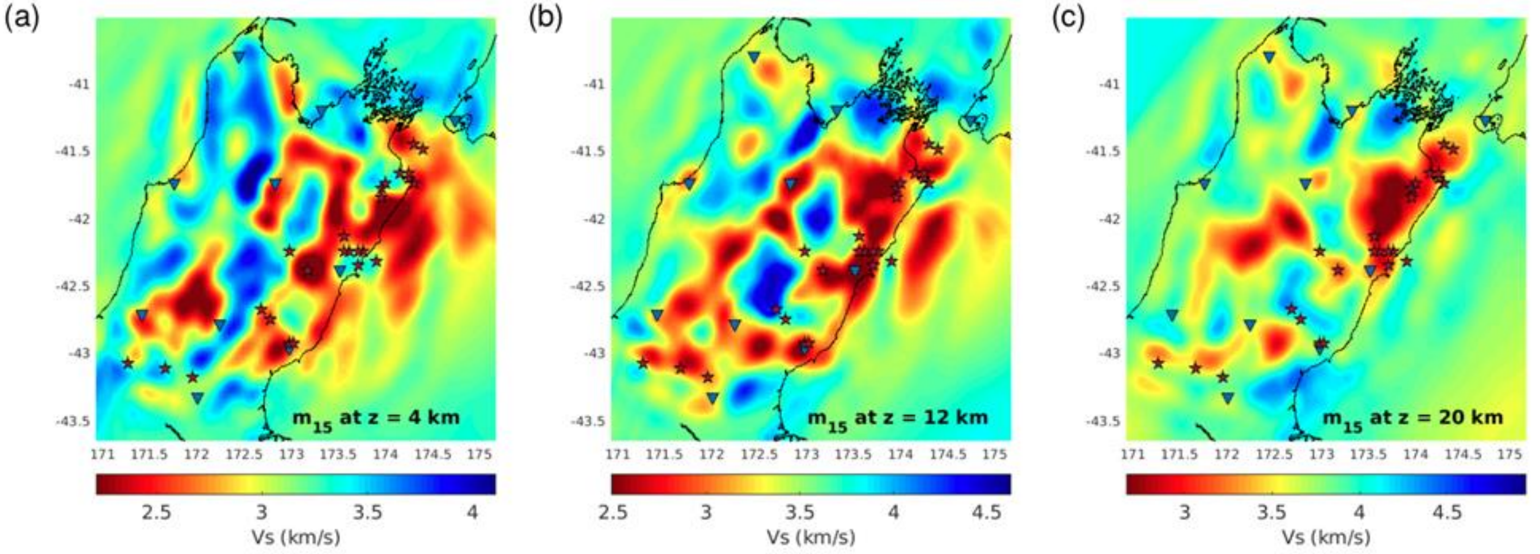

Figure 17: Inverted model after 15 iterations at depth: (a) 4 km, (b) 12 km and (c) 20 km.

Full Waveform Tomography using broadband station data: inverted model assessment

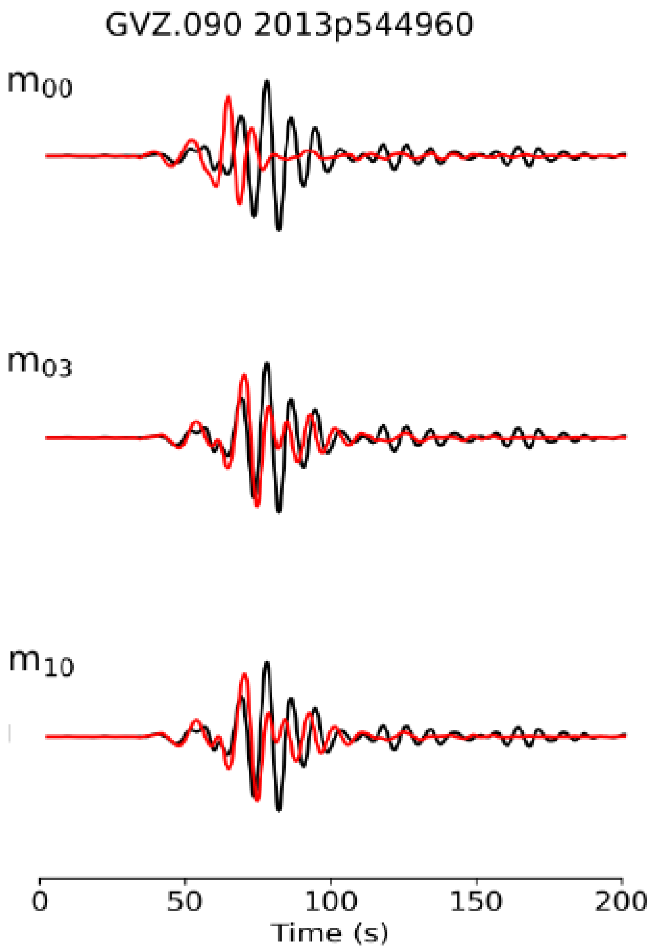

Figure 18: (a) Waveform comparison between observed (black) and simulated (red) data for 3 models: m00, m03 and m10.

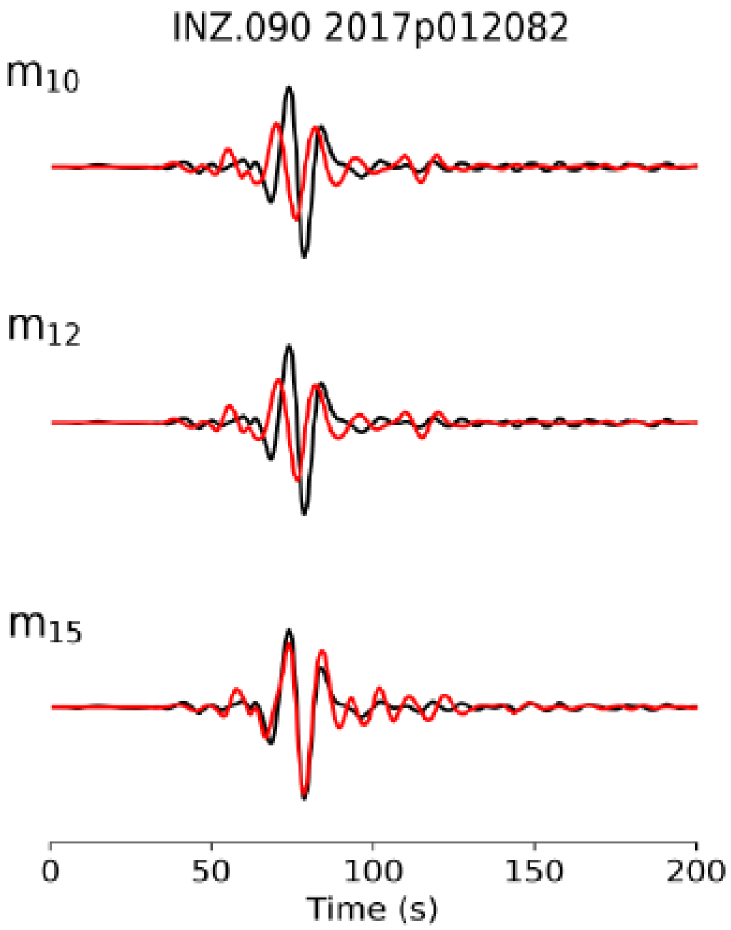

Figure 19: (a) Waveform comparison between observed (black) and simulated (red) data for 3 models: m10, m12 and m15 according to a newly added event.

Full Waveform Tomography using broadband data: inversion starting with different initial NZVM models.

- Eberhart-Phillips NZVM models 2010 and 2020

Figure 20: Initial models: (a) NZVM 2010, (b) NZVM 2020.

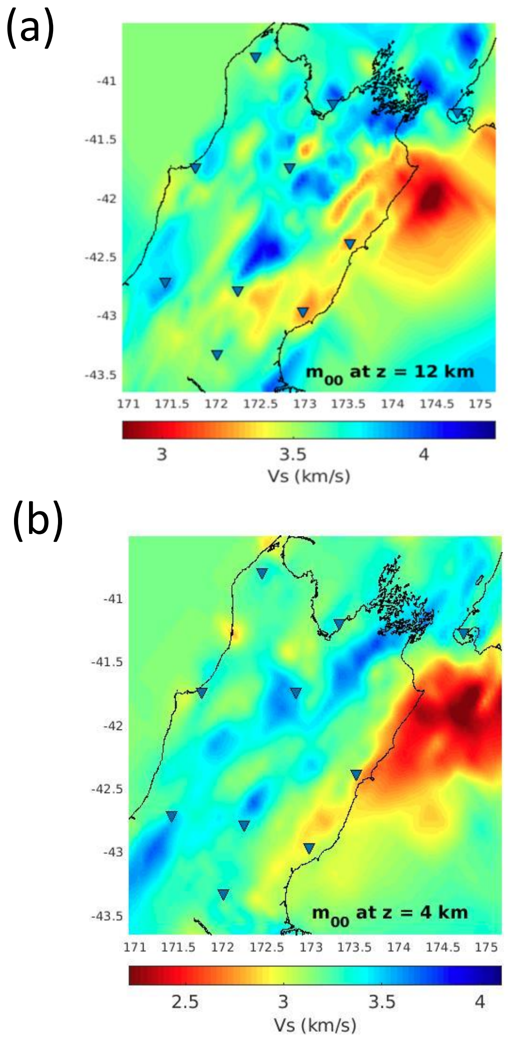

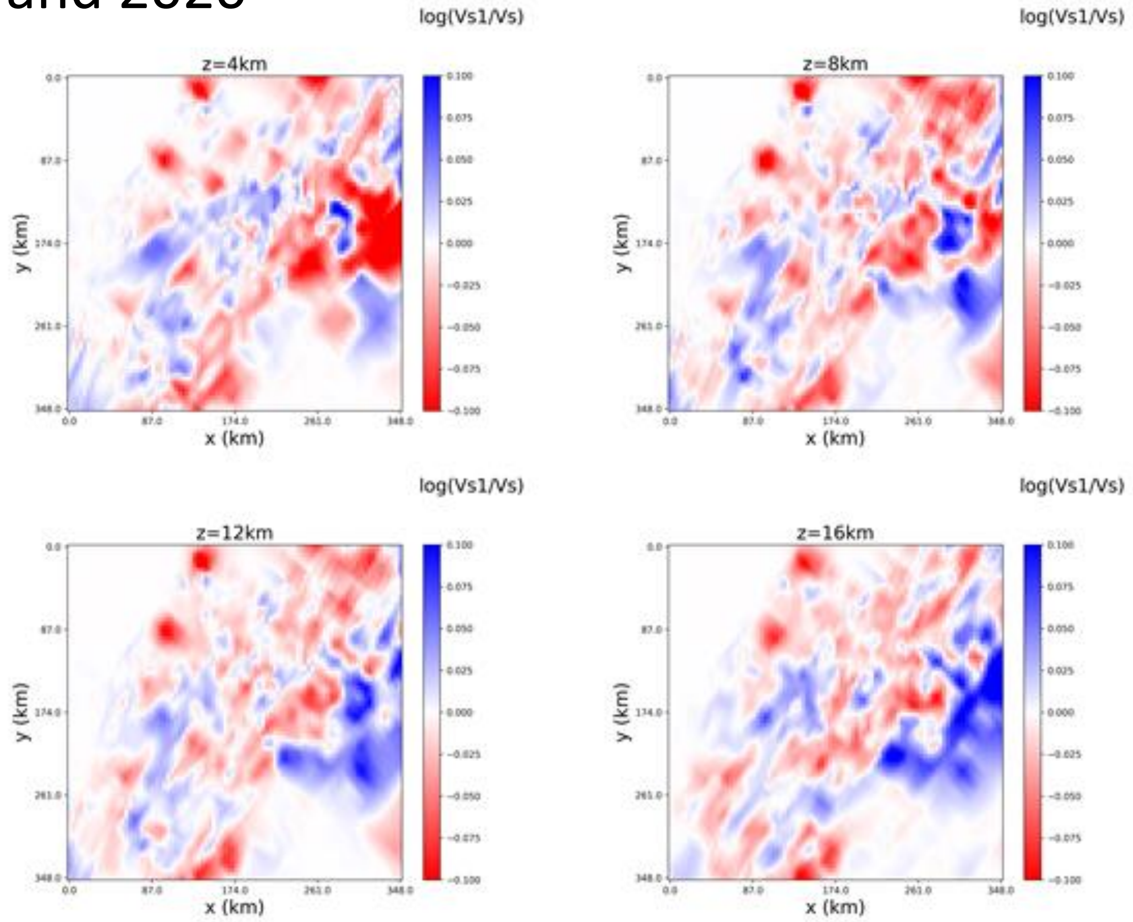

Figure 21: Model change between NZVM 2010 and NZVM 2020 at depth: 4 km, 8 km, 12 km and 16 km.

Full Waveform Tomography using broadband station data: inversion starting with different initial NZVM models

- Inversion using the same observed data set starting with NZVM 2020 and NZVM 2020.

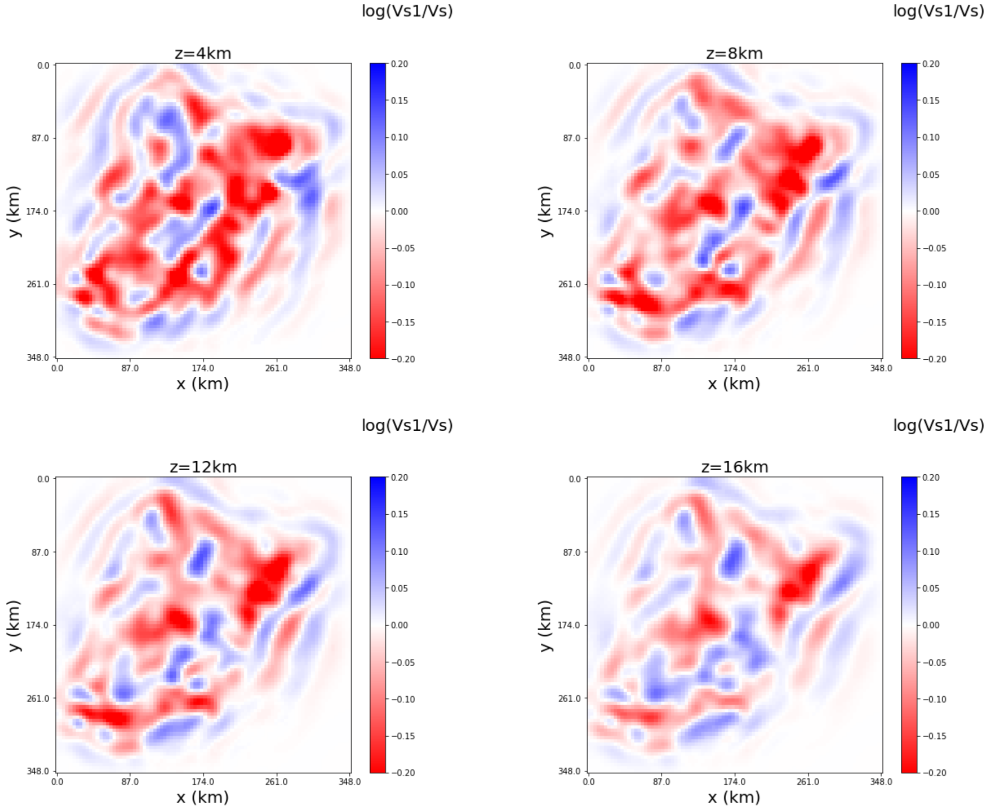

Figure 22: Model change after 10 iterations starting with NZVM 2010 at depth: 4 km, 8 km, 12 km and 16 km.

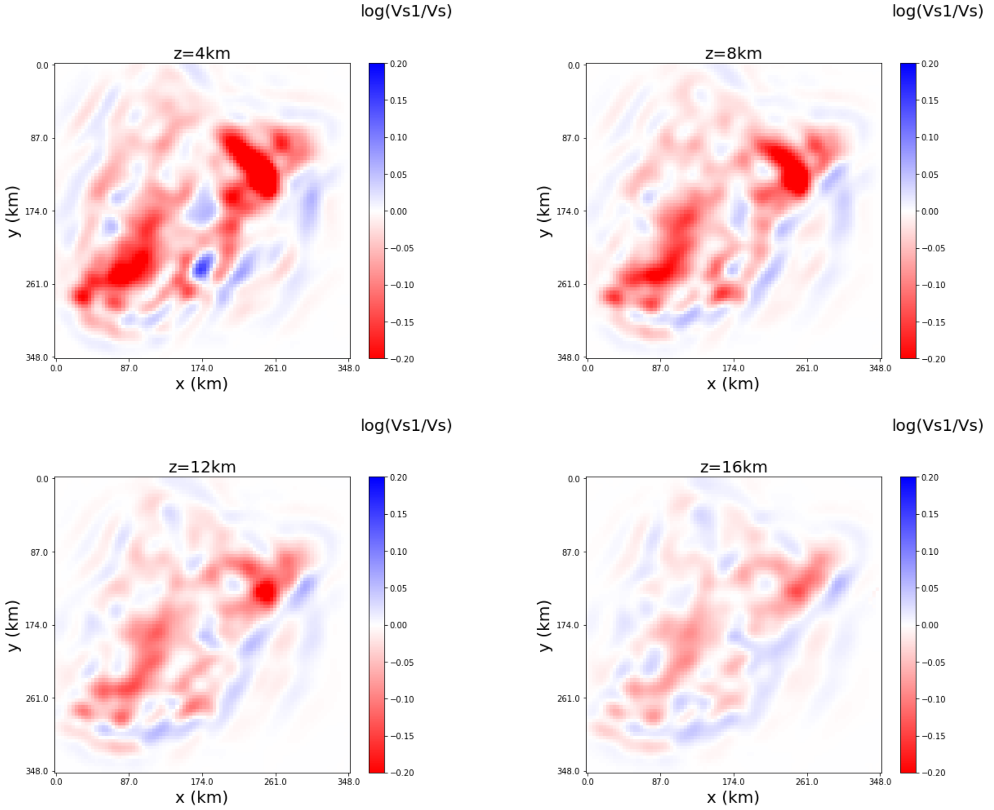

Figure 23: Model change after 10 iterations starting with NZVM 2020 at depth: 4 km, 8 km, 12 km and 16 km.

Full Waveform Tomography using broadband station data: inversion starting with different initial NZVM models

- Misfit and window picked comparison for the two inversion processes.

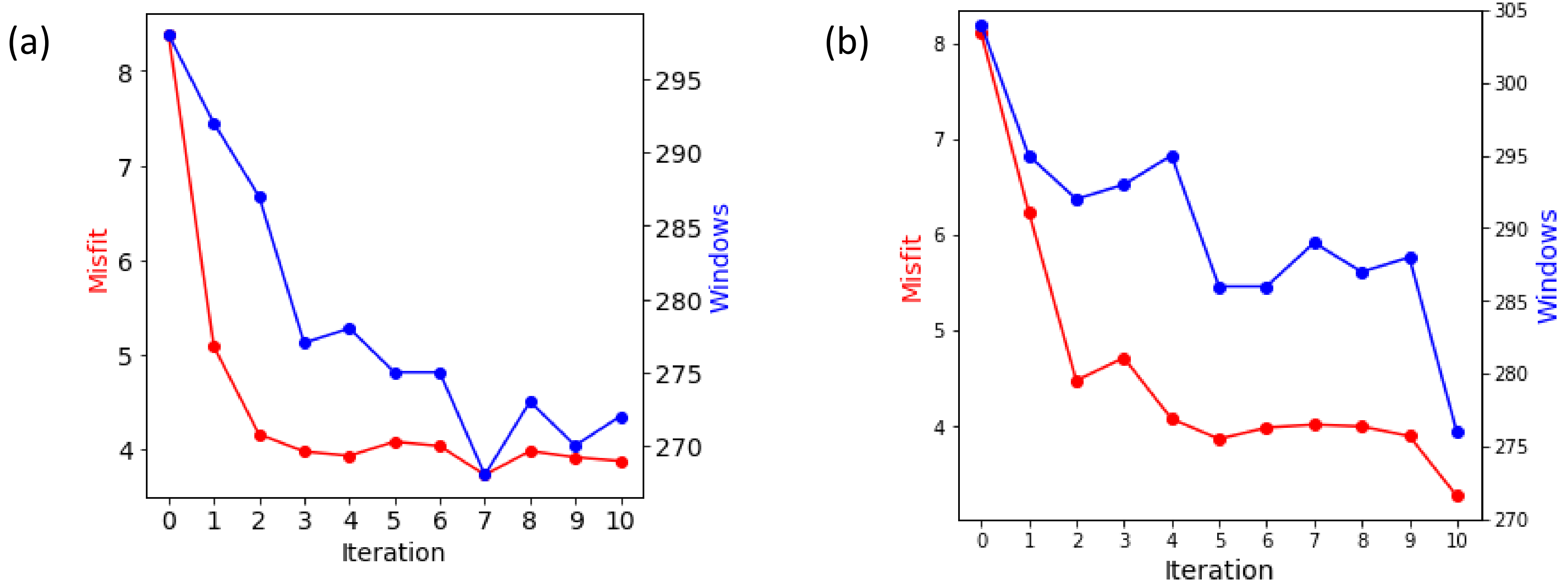

Figure 24: Change of misfit (red) and number of windows (blue) 10 iterations using 13 event data: (a) NZVM 2010 as the initial model, (b) NZVM 2020 as the initial model.

Conclusion on Full Waveform Tomography for the upper South Island region, New Zealand

- The automated workflow has been implemented efficiently on Maui super computer.
- The data processing packages (*Pyflex, Pyadjoint*) are configured for good quality of data selection, segmentation and misfit calculation.
- The checkerboard test has shown the good performance of recovering the checkerboard with a relatively sparse set of stations and events.
- The full waveform inversion of a small number of events (13 events) and 10 broadband station with good spatial distribution can recover large part of the domain for the depths from 0-20 km.
- The further improvement of tomographic inversion can be carried on by adding more events. Choosing a good initial velocity model also has an important impact to the inversion process.

Conclusion on Full Waveform Tomography for the upper South Island region, New Zealand

- Suggestion to improve the velocity model for other NZ wide regions:
  - Revise the CMT solutions of the sources by inversion or relocation.
  - Refine the spatial grid and increase the frequency content of the data included in the inversion.
  - Consider ambient noise data from broadband stations for tomographic inversion.